J. Fluid Mech. (1983), *vol.* 134, *pp.* 311–328
Printed in Great Britain

On the structure and resolution of wall-pressure fluctuations associated with turbulent boundary-layer flow

By GÜNTER SCHEWE†
Max-Planck-Institut für Strömungsforschung, D-3400 Göttingen, Federal Republic of Germany

(Received 23 August 1982 and in revised form 15 March 1983)

In a wind tunnel designed for flow-acoustic measurements, the wall-pressure fluctuations beneath a turbulent boundary layer have been investigated. The measurements were carried out with variously sized pressure transducers ($19 \leqslant d^+ \leqslant 333$) and with an array of four small transducers (separation distance $\Delta x^+ = 75$). It is shown that the dimensionless diameter $d^+ = 19$ of the transducers is sufficient to resolve the essential structures of the turbulent pressure fluctuations. The power spectrum $\Phi(\omega^+)$ measured with the smallest transducer $d^+ = 19$ partly exhibits power-law decay $\Phi \sim \omega^{-\frac{7}{3}}$, which has been theoretically predicted for locally isotropic turbulence. By visual analysis and signal averaging in the time domain, pressure structures with high amplitudes could be detected which have the shape of short wavetrains or pulses. Their characteristic frequency and longitudinal wavelength have the mean values $\omega^+ = 0.52$ and $\lambda^+ = 145$ respectively, and their mean convection velocity amounts to $u_c/u_\infty = 0.53$. It was calculated from the measured probability density that these characteristic structures play an important role, although the probability of their occurrence is low. The sources of these wall-pressure structures can be located in the buffer layer of the boundary layer.

1. Introduction

Wall-pressure fluctuations beneath a turbulent boundary layer are related to the fluctuations of the velocity field in the boundary layer. It is possible to obtain information about the boundary layer itself, without disturbing the flow by measuring probes, by measurement of the wall pressure, which is an integral value of the velocity field. A great part of the work done in this field is reviewed by Willmarth (1975).

An important parameter for an experimental investigation is the ratio between the pressure-transducer size and the smallest important lengthscale of the flow. This ratio should be as small as possible. In most known previous investigations this ratio was rather large, so that the resolution for typical turbulent structures with high wavenumbers was poor. Attempts to improve the resolution by using pinhole (Blake 1970) or orifice microphones (Hodgson 1962) can lead to disturbances of the flow at the wall. These effects have been proved by Bull & Thomas (1976) in a comparative investigation. Because of this, a necessary condition for investigation of small-scale structures is the improvement of the resolution, whereby the pressure transducer has to form an integral part of the wall.

As a consequence, new small pressure transducers have been developed, which fulfil these requirements. Moreover, by applying variously sized transducers the effect of

† Present address: Inst. f. Aeroelastik der DFVLR-AVA Göttingen, D-3400 Göttingen.

spatial low-pass filtering on the statistical properties will be studied. In this context the following question will be answered: which value of the non-dimensionalized transducer diameter is necessary so that the essential structures of the turbulent boundary layer can be resolved?

In several recent investigations, the occurrence of coherent structures in turbulent boundary-layer flow has been demonstrated, as summarized by Cantwell (1981). In addition reference is made to the work performed by Eckelmann *et al.* (1977), Hofbauer (1978) and Kreplin & Eckelmann (1979) in the Göttingen oil channel. This work was concentrated on the coherent structures in the wall region.

The present work was conducted in the wind tunnel in which Emmerling (1973) and Dinkelacker *et al.* (1977) investigated wall-pressure structures by means of an optical method. Furthermore, this work is concerned with the investigation of the statistical properties of the characteristic wall pressure structures by signal averaging and visual analysis in the time domain. In addition, relations between the characteristic wall-pressure structures and the phenomena occurring in the buffer layer will be sought.

2. The wind tunnel and its flow parameters

The wind tunnel was especially designed for flow-acoustic measurements by Emmerling, Meier & Dinkelacker. A detailed description is given by Emmerling (1973) and Dinkelacker *et al.* (1977). The flow is driven by suction so that the measurements are not disturbed by the noise of a fan. For the purpose of achieving a constant flow velocity an adjustable sonic nozzle is built between the vacuum vessel and the wind tunnel. The test section has a length of 2.4 m and a rectangular cross-section of 0.2×0.1 m. The walls are made of cast aluminium for reduction of structurally inherent noise. Between the test section and the sonic nozzle is a first sound absorber for damping the sound radiating from the sonic nozzle into the test section. From the nozzle the air flows with the velocity of sound into a second absorber and then finally into the vacuum tank ($V = 130$ m^3). The entire tunnel is suspended by springs in order to decouple the tunnel from the building. The coordinate system is chosen such that the x-axis points in the flow direction; the positive y-axis is normal to the wall where the pressure transducers are mounted. The z-axis is perpendicular to the (x, y)-plane, forming a right-handed system. On the flat walls of the wind tunnel, a turbulent boundary layer forms as on a flat plate. At the same x- and z-position where the pressure transducers are mounted, the velocity distribution and the turbulence-intensity distribution were measured (figures 1 and 2) by means of a hot-wire probe. The centreline velocity $u_\infty = 6.3$ m/s was chosen to be the same for all measurements, which is a compromise between two contrary requirements. On the one hand the flow velocity should be large in order to get pressure fluctuations with high intensity, and on the other hand a better spatial resolution of the pressure transducer is achieved in the case of lower flow velocity (while the transducer size remains constant). The reason for this is the fact that the characteristic lengthscales of turbulent flow increase with decreasing flow velocity. The flow is characterized by the following values: velocity outside the boundary layer $u_\infty = 6.3$ m/s; boundary-layer thickness $\delta = 30$ mm; displacement thickness $\delta^* = 4.6$ mm; momentum thickness $\theta = 3.3$ mm; shear velocity $u_\tau = 0.28$ m/s; wall shear stress $\tau_w = 0.09$ Pa; Reynolds number with respect to θ $Re_\theta = 1400$; sublayer lengthscale $\nu/u_\tau = 54$ μm.

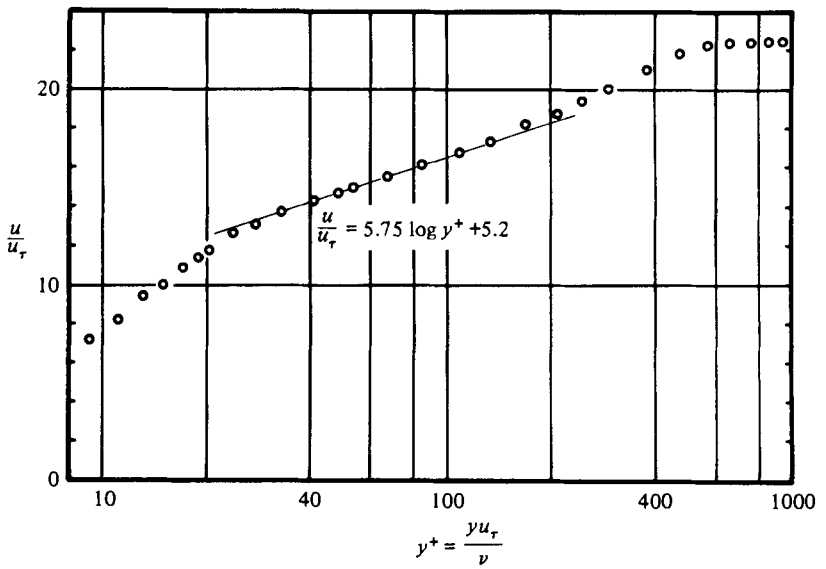

FIGURE 1. Velocity distribution in the test section.

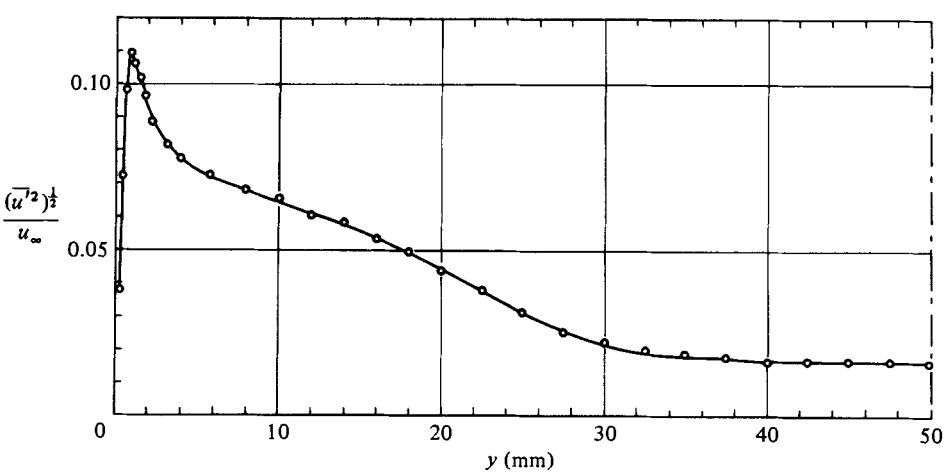

FIGURE 2. Turbulence-intensity distribution in the test section.

3. Pressure transducers

The requirement for good spatial resolution and sensitivity in our experiments makes pressure transducers commonly used in fluid dynamics and acoustics either too insensitive or too large. Therefore small transducers of the Sell type were developed, the working principle of which can be briefly described as follows: the Sell transducer (see e.g. Kuhl, Schodder & Schröder 1954) belongs to the category of electrostatic microphones which consist of a light conductive membrane and a counterelectrode. This combination works like a capacitor whose fluctuations of capacity created by sound waves can be transformed by appropriate electronics into fluctuations of voltage. In the case of the Sell transducer, as illustrated in figure 3, the capacitor comprises a rough counterelectrode and a foil of plastic material with a thin metal

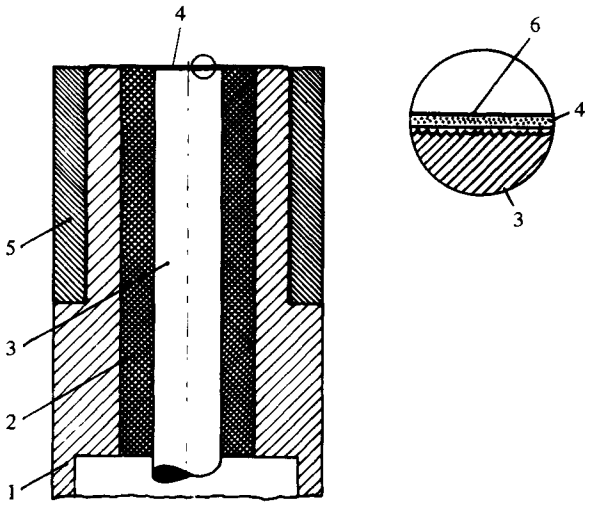

FIGURE 3. Cross-section sketch of the pressure transducer: housing (1), insulator (2), counterelectrode (3), foil (4), ring (5), metallic layer on foil (6).

layer. The foil is stretched over the counterelectrode such that the plastic is interposed between the conductors. Thus the flexible metal layer and the solid counterelectrode form the two plates of the capacitor. Because the foil lies on the minute elevations of the rough counterelectrode, an air cushion results between the counterelectrode and the foil, so that small movements of the membrane are allowed. The sensitivity and the frequency response can be influenced by an appropriate choice of the roughness of the counterelectrode. The greater the roughness, the higher the sensitivity and the lower the cutoff frequency, and vice versa. These properties made it possible to obtain sufficient sensitivity for the measurement of small pressure fluctuations, whereby the frequency response is chosen such that the essential frequencies of turbulence remain undamped. It was intended to produce a transducer diameter approximately equivalent to the thickness of the viscous sublayer. For a flow velocity of about $u_\infty = 6$ m/s, this requirement demands a diameter of $d \approx 1$ mm and a sensitivity of the same magnitude as the smallest available commercial microphone (Bruel & Kjaer $\frac{1}{8}$ in.).

The main problem of producing such a small transducer is to achieve a defined roughness of the counterelectrode, because this roughness determines the properties of the transducer. The problem was solved by etching the individual brass counterelectrodes under constant conditions. The construction of the transducer is schematically illustrated in figure 3. The outer diameter of the transducer is $D = 4$ mm and the diameter of the sensing area is $d = 1$ mm. When the housing (1), insulator (2) and counterelectrode (3) are assembled, a thin foil (thickness = 2 μm) is stretched over the front face of the transducer. This foil (4) is held by the outer ring (5). Lastly, the entire front face is coated with a thin gold layer (6). The preamplifiers for the transducers were especially developed and they work as a high-frequency bridge circuit with a phase-sensitive discriminator. More details about the properties and production of these transducers are given by Schewe (1979).

In addition four Bruel & Kjaer condensor microphones (1, $\frac{1}{2}$, $\frac{1}{4}$ and $\frac{1}{8}$; Types 4144, 4134, 4136 and 4138) were used in order to investigate the effect of spatial low-pass filtering. Special adapters were mounted on the two larger B & K microphones

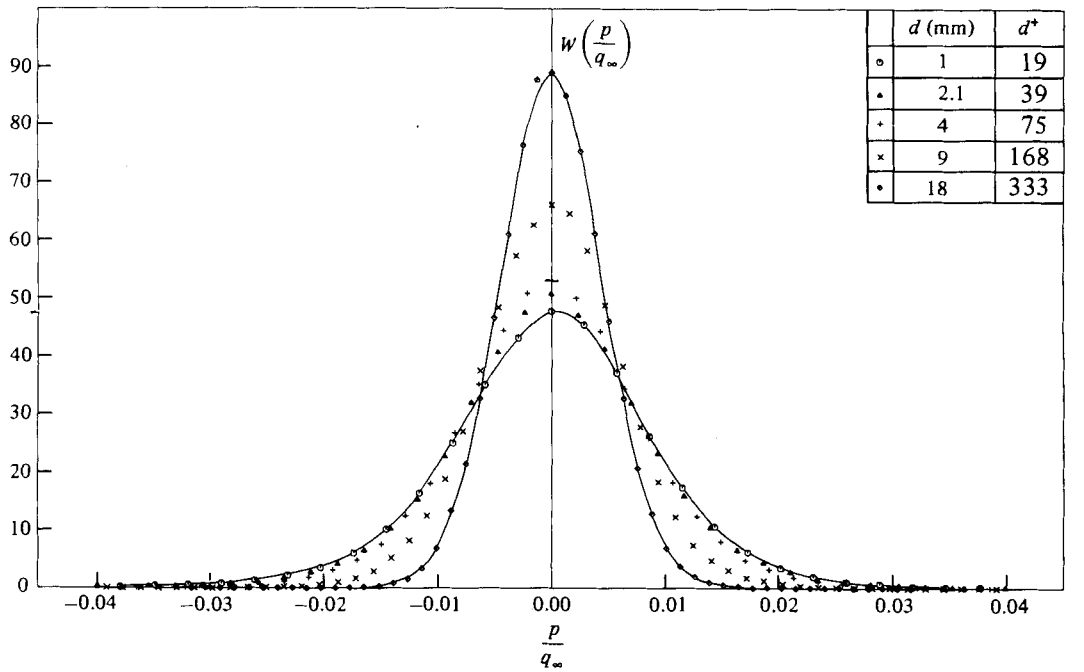

FIGURE 4. Probability density distributions recorded with variously sized pressure transducers.

(1, ½ in.); which provided the most nearly continuous transition from the wind tunnel wall to the membrane surface of the microphone.

Evaluation of the measurements was undertaken mainly by a digital computer (PDP 15) equipped with an analog-to-digital converter (8-channel). The single-channel measurements were given directly into the A/D converter system. For 4-channel measurements, an Ampex FR 1300 tape recorder was used for making a frequency transformation (1:2) which was necessary to fulfil the 'sampling theorem'. The power spectra and the r.m.s. values were measured directly by a real-time analyser (General Radio Type 1925/1926).

4. Probability distribution and its moments

In figure 4 the probability density distribution of the pressure amplitudes is illustrated, measured with five variously sized pressure transducers. The pressure amplitudes p relate to the dynamic pressure q_∞ of the free stream, and the probability distributions are normalized in such a way that the area under each curve has the value 1. The considerable influence of the pressure transducer diameter is evident in the continuous expansion of the probability distribution as the transducer diameter is decreased, i.e. the probability of the occurrence of higher pressure amplitudes increases as the transducer diameter decreases.

The moments of the probability density distribution skewness and flatness factor were calculated from the same data, and are illustrated in figure 5 as functions of the pressure transducer diameter $d^+ = du_\tau/\nu$. The second moment, the r.m.s. value, is isolated and discussed in § 5.

The flatness factor decreases continuously from 4.9 for the smallest transducer to a value of 3.1 for the largest transducer. The skewness factor is negative for the two

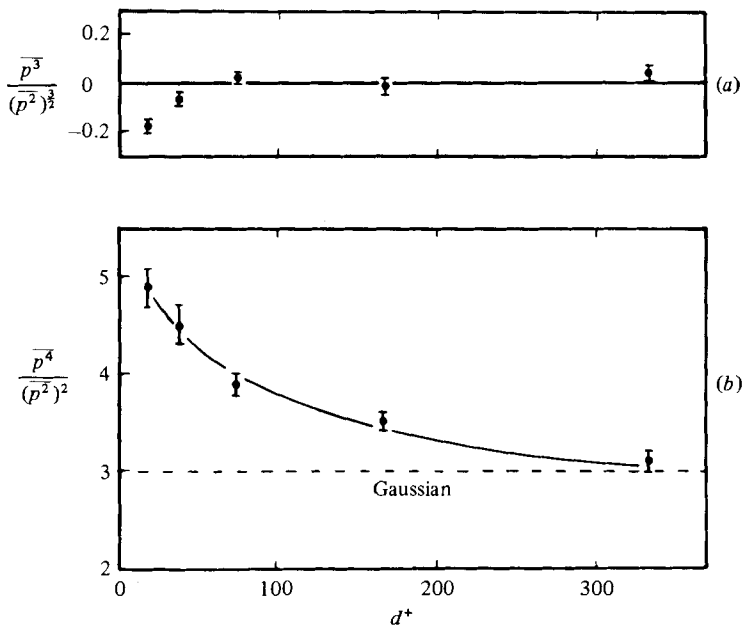

FIGURE 5. Dependence of 3rd and 4th moment skewness (*a*) and flatness factor (*b*) upon the transducer size.

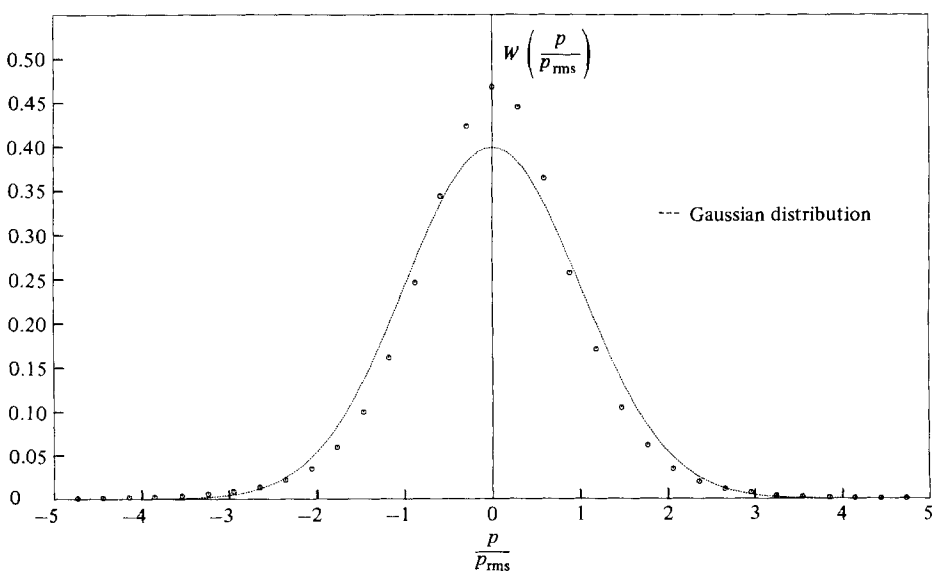

FIGURE 6. Probability density distribution of the wall-pressure fluctuations ($d^+ = 19$).

smallest transducers, indicating asymmetry in the probability density distribution. Indeed, the probability of such an occurrence of higher negative pressure amplitudes is somewhat greater than the occurrence in inversely similar pressure amplitudes. This slight asymmetry is barely detectable in figure 6, in which the probability density distribution W, recorded by the smallest pressure transducer ($d^+ = 19$), is particularly accentuated in comparison with a Gaussian distribution. The pressure amplitudes are thus normalized to the r.m.s. value. Under close inspection, the probability density

$\frac{p_{th}}{p_{rms}}$	$W(p < -p_{th})$ %	$W(p > p_{th})$ %	$W(\|p\| > p_{th})$ %	Gaussian $W(\|p\| > p_{th})$ %
0	49	51	100	100
1	13.5	13.5	27	32
2	2.7	2.3	5.0	4.6
3	0.6	0.4	1.0	0.27
4	0.2	0.1	0.3	0.01

TABLE 1. Calculation of the probability that the wall pressure amplitude p exceeds the threshold p_{th}

at high negative amplitudes (e.g. $-3p/p_{rms}$) is considerably greater than at correspondingly high positive pressure amplitudes. To emphasize this slight asymmetry, the integrals over a larger area of probability density function were calculated. The probability $W(a \leqslant p \leqslant b)$ was calculated directly from the time function $p(t)$, such that the wall pressure amplitude exceeds the positive threshold or falls below the negative threshold. This calculation is equivalent to the determination of the area under the probability density with the threshold as the limit of integration (the other limits are $+\infty$ and $-\infty$, respectively):

$$W(a \leqslant p \leqslant b) = \int_a^b W(p)\, dp.$$

If we have the negative threshold p_{th} then $a = -\infty$ and $b = -p_{th}$ and vice versa.

In table 1 these calculated probabilities are recorded for the smallest pressure transducer ($d^+ = 19$). As can be seen, the greater probability density for the occurrence of high negative pressure amplitudes begins at a threshold of approximately $2p_{rms}$ and increases further for higher thresholds. Another interesting result can be taken from this calculation. The probability that the amplitude exceeds the positive or negative threshold $|p_{th}|$ is recorded in the 3rd column. When we consider for example $W(|p| > 3p_{rms})$ then the probability amounts to 1 %, which means that the threshold $p_{th} = \pm 3p_{rms}$ is exceeded for 1 % of the time. This value seems to be very low, but we will see later that the events which fulfil this condition play an important role in the wall region of the turbulent boundary layer. For the sake of comparison a corresponding calculation has been made for a Gaussian distribution (4th column). Finally the largest wall-pressure amplitudes observed were up to $p_{peak} = \pm 7p_{rms}$.

Another significant characteristic is that the low and extremely high amplitudes occur more frequently in the case of wall-pressure fluctuations than in a process obeying the Gaussian distribution function, which is characterized by the high flatness factor. This characteristic indicates an intermittent process concerning wall pressure measured with small pressure transducers, where time intervals with relatively large fluctuations follow periods of small fluctuations. This fact was also observed by Emmerling (1973), who used a different method of investigation.

In order to give an impression of the statistical significance of the non-Gaussian effects, error bars are included in figure 5, which were calculated as follows: the entire time record ($T = 30$ s) was divided into 12 subrecords. Thus the variance of the mean values could be calculated, which are represented by the error bars. The accuracy when measuring higher statistical moments is mainly limited by the finite integration time. Nevertheless it is obvious that the non-Gaussian effects are significant.

Because seemingly typical characteristics of turbulent fluctuation quantities

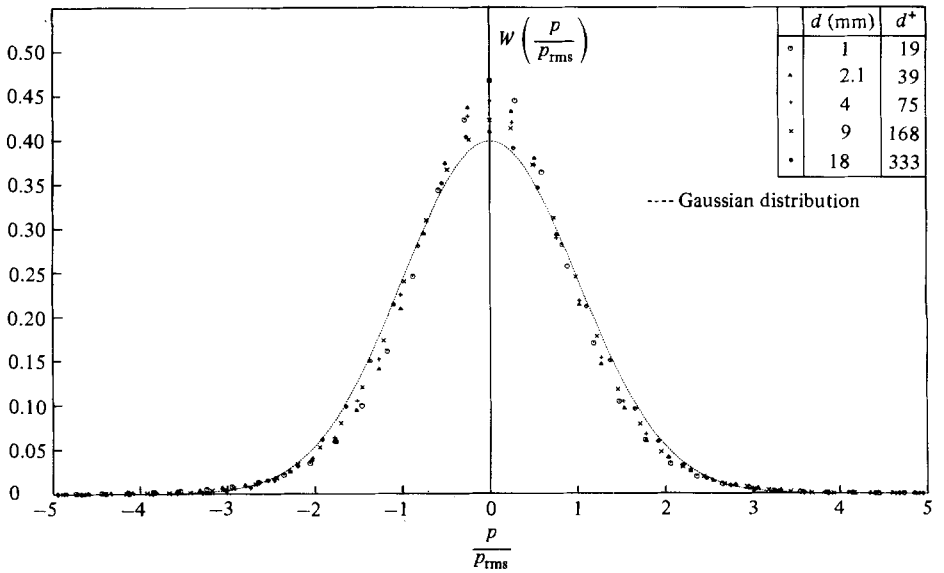

FIGURE 7. Probability distribution from figure 4, but normalized to their corresponding r.m.s. value.

appear when the probability density distribution deviates from the Gaussian distribution, the five probability distributions are pictured again in figure 7. As opposed to figure 4, all the distributions are now compared with the Gaussian distribution and normalized to the corresponding r.m.s. value. Obviously, the deviation of the measured distribution from the Gaussian distribution decreases as the pressure transducer diameter is increased. Except for the somewhat higher probability density for small amplitudes, the probability distribution measured with the largest microphone is in good agreement with the Gaussian distribution. This tendency is confirmed by the skewness and flatness factors, which are determined directly from the time functions. As shown in figure 5, these factors approach 0 and 3 respectively for increasingly large pressure transducers (with Gaussian distribution, skewness is 0 and flatness is 3). From the facts stated here the following hypothesis may be made.

If the diameter of a circular pressure transducer is increased while turbulent wall-pressure fluctuations are measured under a boundary-layer flow, then the probability distribution of the pressure amplitudes for 'large' diameters converges to a Gaussian distribution. The following reasons may be given in support of this hypothesis. The central limit theorem of probability theory reads: 'The sum of an infinite number of independent stochastic processes with mutually equivalent, arbitrary probability distribution has a Gaussian probability density distribution.' If such an occurrence is observed on the pressure transducer at any fixed time, it is conceivable that the instantaneous total pressure on the transducer surface is the sum of the pressures from several individual pressure structures. Further, if these individual pressure structures are statistically independent from each other and the number of the pressure structures is large enough ('larger pressure transducers'), then the central limit theorem holds true, i.e. the sum of the individual pressure structures obeys a Gaussian distribution.

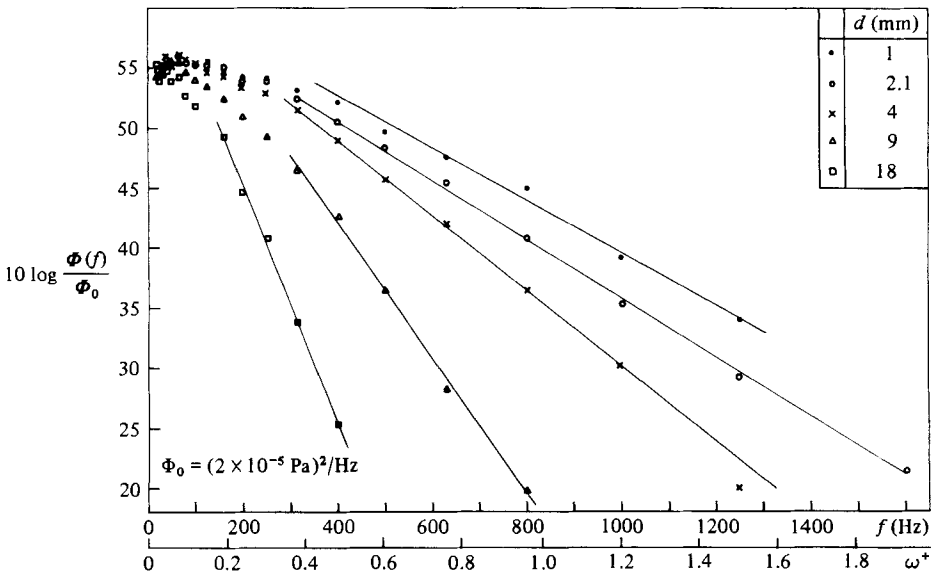

FIGURE 8. Power-spectral densities recorded with variously sized pressure transducers.

5. Power spectra and r.m.s. values

In figure 8, power spectra of the wall-pressure fluctuations are illustrated, recorded by microphones of various sizes. The non-dimensional angular frequency $\omega^+ = \nu/u_\tau^2$ is obtained by using the friction velocity u_τ and the kinematic viscosity ν. Clearly, the power-spectral density is approximately equal for all spectra only at frequencies up to about 30 Hz. At higher frequencies the spatial low-pass filtering causes a weakening of the larger wavenumbers, implying that the length of the pressure structures is as large as or smaller than the diameter of the pressure transducer. In the spectra recorded with the three smaller microphones, a slightly pronounced maximum appears at about 60 Hz ($\omega^+ = 0.07$). Common to all spectra seems to be the exponential decay at high frequencies unnoticed in earlier investigations. It should be noted that the spectrum taken with the smallest microphones deviates slightly from the exponential decay. This will be discussed later. Characteristic frequencies can be determined as slope constants $\omega_{SL} = \omega_{\frac{1}{2}}/\ln 2$ for each spectrum from its high-frequency part. As the microphone diameter is decreased, the slope constant increases, indicating a steeper decay of the spectrum. This conclusion poses the question as to whether the spectra of other investigations exhibit such an exponential decay as well. As a result of an evaluation of the data measured by Emmerling (1973), Willmarth & Roos (1965) and Bull & Thomas (1976), the spectra show also an exponential decay, evidently typical for wall-pressure spectra. The slope constants expressed as characteristic frequencies were non-dimensionalized corresponding to the frequency scale of the spectra with wall variables ($\omega_{SL}^+ = \omega_{SL}\nu/u_\tau^2$) and are illustrated in figure 9.

The slope constants obtained from the spectra of the three smaller microphones lie practically in a straight line. An extrapolation to the diameter $d^+ = 0$ yields a value of $\omega_{SL}^+ = 0.26$. Even for the slope constants obtained in three other investigations with a different wind tunnel configuration (Willmarth & Roos 1965; Bull & Thomas 1976) and with different Regnolds numbers (Emmerling 1973), a smooth curve drawn

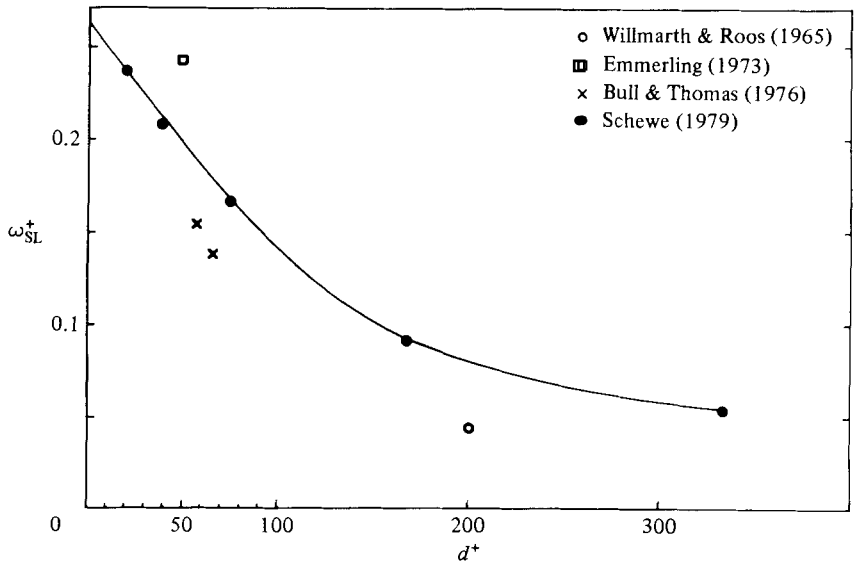

FIGURE 9. Normalized slope constants ω^+_{SL} of the power-spectral densities from figure 8.

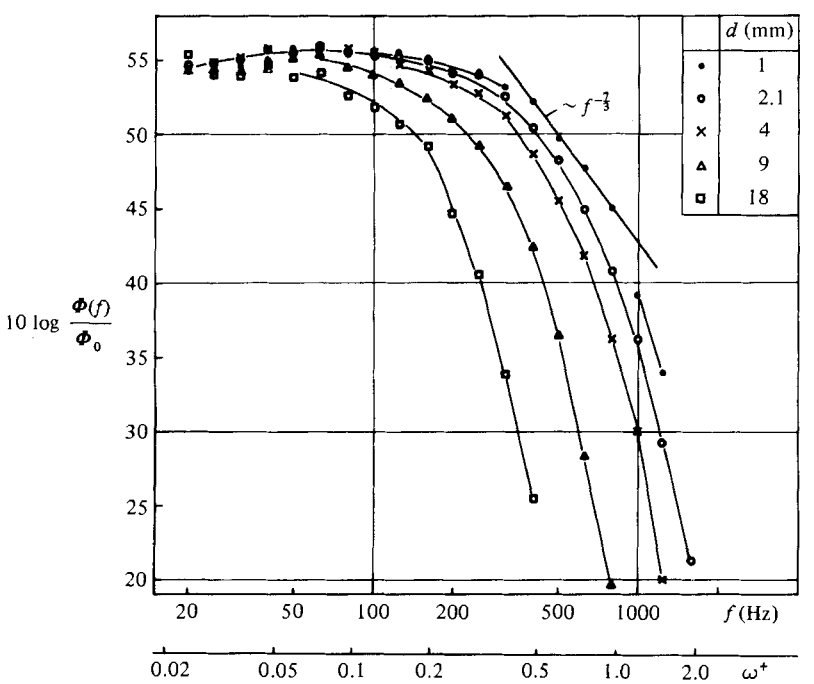

FIGURE 10. Data from figure 8 plotted with logarithmic frequency scale.

through these values obviously gives a good fit. Thus the extrapolated value ω^+_{SL} seems to achieve a certain general validity.

As mentioned above, the high-frequency part of the spectrum taken with the smallest microphone shows a slight deviation from exponential decay such that further inspection is suggested. Thus in figure 10 all five power spectra are plotted

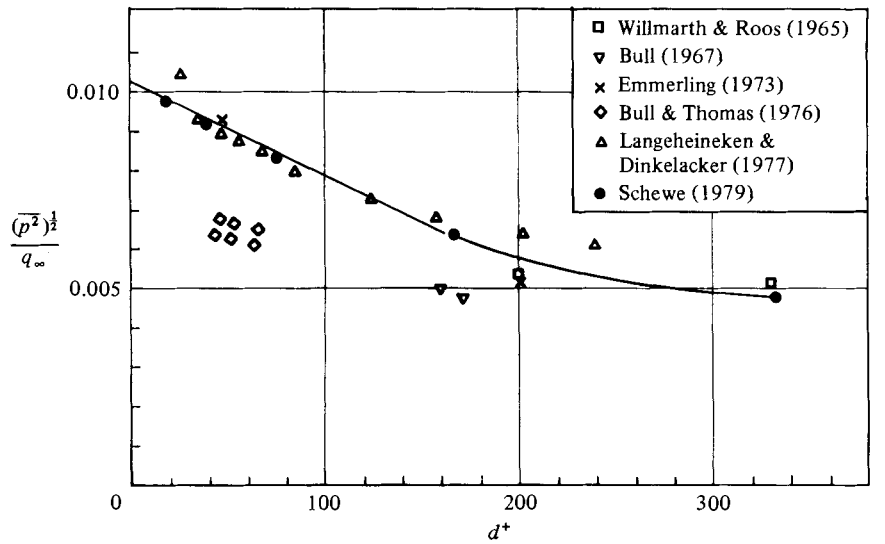

FIGURE 11. Dependence of the normalized r.m.s. value upon the normalized transducer diameter.

with a logarithmic frequency scale. It is obvious that for $d^+ = 19$ the power law $\Phi(\omega^+) \sim (\omega^+)^{-\frac{7}{3}}$ gives a good fit for the range $0.4 \lesssim \omega^+ \lesssim 0.8$. This power law for the decay of the power spectral density was theoretically predicted for locally isotropic turbulence (see e.g. Monin & Yaglom 1975). These findings suggest the conclusion that the exponential decay of the spectra is a consequence of the limited spatial resolution of the pressure transducers used.

Apart from the frequency distribution, the integral over the power spectrum (the r.m.s. value) is of great importance, because it is a measure of the intensity of a process. Figure 11 illustrates the measured dependence of the wall pressure fluctuation r.m.s. value on the normalized pressure transducer diameter together with the results of other authors (symbol ●). Here the diameter was non-dimensionalized with the length ν/u_τ characteristic for the wall region, and the r.m.s. value of the pressure fluctuations with the dynamic pressure q_∞ of the free stream. The diameter is varied in this investigation from $d^+ = 19$ to $d^+ = 333$ while the flow parameters remain unchanged. Clearly the normalized r.m.s. value of the wall-pressure fluctuations increases from about 0.5% to 1% as the diameter of the pressure transducer is decreased. The values measured in this investigation for diameters under $d^+ \approx 200$ lie on a straight line, so that an extrapolation to the diameter $d^+ = 0$ is clearly suggested. The extrapolated value is 4% greater than the value measured with the smallest pressure transducer, which indicates good agreement in view of the measuring accuracy. This result confirms the conclusion that pressure transducers of diameter $d^+ \approx 20$ are able to resolve the pressure structures essential to turbulence.

In comparing these results with those of other investigations (fig. 11), measurements performed with pinhole microphones are not taken into consideration, because their use can lead to disturbances in the high-frequency region of the spectrum, as proved by Bull & Thomas (1977). The results from Bull & Thomas and from Bull (1967), performed with a piezoelectric crystal element, were about 20–30% lower than the present ones using the same dimensionless diameter, while the results obtained by Willmarth & Roos (1965) conform to the general trend. The cause for these deviations

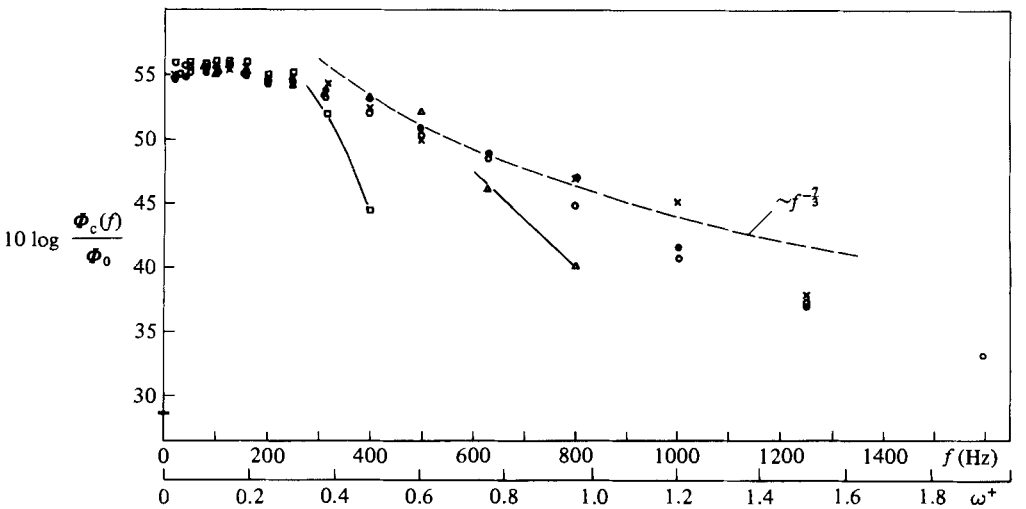

FIGURE 12. Corrected power-spectral densities $\phi_c(f)$ based on the data from figures 8 and 10.

may be attributed to the different sensitivity distribution over the diameter of the pressure transducer, or possibly to the particular wind-tunnel features. From the results of Langeheineken & Dinkelacker (1977) it is noted that the investigation was performed in fully developed pipe flow where the diameter of the pressure transducer remained constant while the flow parameters were changed. The agreement between the present results and theirs is surprising. It allows the assumption that the characteristic features of the wall pressure fluctuations are mainly influenced by the action in the wall region.

6. Application of a transducer resolution correction

The present set of measurements with various-sized pressure transducers ($19 \leqslant d^+ \leqslant 333$) allow a check of transducer resolution correction methods. Corcos (1963, 1967) calculated the transducer resolution correction to the power spectrum in terms of the similarity parameter $\omega r/u_c(\omega)$, where r is the radius of the pressure-sensitive area of the transducer. As the frequency-dependent convection velocity $u_c(\omega)$ was not measured in the present investigation, the data of Corcos (1963) were used. The corrected spectra are illustrated in figure 12.

It is evident that the high-frequency part of the spectra measured with the two larger transducers ($d^+ = 168, 333$) is attenuated compared with the spectra measured with smaller transducers ($d^+ = 19, 39, 75$). Inspection of the data reveals that the correction according to Corcos is too small for $\omega r/u_c \gtrsim 4$. By integrating the corrected power spectra, the individual r.m.s. values were calculated. The correction factors $F = (p_{rms})_{corr}/(p_{rms})_{mea}$ and the corrected r.m.s. values are recorded in table 2. The correction to p_{rms} ($d^+ = 19$) measured with the smallest transducer is almost negligible ($F = 1.07$) considering the limitations of a correction method and taking into account measuring accuracy. The results (table 2) show that for $19 \leqslant d^+ \lesssim 168$ the corrected r.m.s. values reach approximately the value of $p_{rms}/q_\infty = 0.0102$, which was found by extrapolation to zero transducer size (figure 11). Thus it can be concluded that, based on the present experiments, the Corcos correction can predict the increase of p_{rms}/q_∞ with decreasing d provided that $d^+ \lesssim 160$. The

Pressure transducer	d^+	p_{rms}/q_∞ Measured	Corrected	F
Sell-type	19	0.0098	0.0105	1.07
$\frac{1}{8}$ in. B. & K.	39	0.0093	0.0103	1.12
$\frac{1}{4}$ in. B. & K.	75	0.0084	0.0108	1.29
$\frac{1}{2}$ in. B. & K.	168	0.0064	0.0101	1.58
1 in. B. & K.	333	0.0046	0.0088	1.91

TABLE 2. Measured and corrected r.m.s. pressures

correction is too small for $d^+ \gtrsim 160$. As mentioned above, the range of validity is limited by the condition $\omega r/u_c \lesssim 4$. As Corcos used measured data for his calculations, it is possible that the experimental input is partly responsible for the limited validity of his correction method.

7. Analysis of time functions

7.1. *Visual analysis*

Aside from statistical analyses obtained by long-time averaging which indicate the individual processes of turbulent flow only partially, it is of particular interest to study the time functions themselves in order to find coherent structures with similar appearances which most probably appear repeatedly.

Segments of the time functions of an array of four consecutive pressure transducers which are orientated in the direction of the flow are represented in figures 13 and 14. The pressure amplitudes of all time functions are normalized to the r.m.s. value; their separation is $\Delta x = \xi = 4$ mm ($\xi^+ = 75$).

Although a visual analysis is often somewhat subjective, certain observations should be noted which were made during the study of many time functions.

(*a*) The similarity between the four time functions (except for a small time delay) indicates nearly frozen structures which move with convection velocity u_c in the boundary layer.

(*b*) The wall-pressure fluctuations are a very intermittent process, where relatively short time segments with large fluctuations follow long time segments with small fluctuations, as follows also from the probability distribution (figure 6).

(*c*) Events that have a maximum amplitude exceeding approximately $5p_{rms}$ (events E_1, E_3 and E_4 in figures 13 and 14) grow and decay much faster than such events as E_2, E_5 and E_6. These events have maximum amplitudes of about $3p_{rms}$, and the change of amplitude over the distance $225\nu/u_\tau = 2.6\delta^*$ is small.

In most cases, the events with high amplitude have the shape of short wavetrains or pulses, so that the determination of a characteristic time T_{ch} seems logical. The time of one oscillation period was determined for all events exceeding the threshold $\pm 3p_{rms}$. This threshold amplitude is indicated in figures 13 and 14 by a dotted line. Determination of the characteristic times proved to be quite simple since marked extremes are always evident. The statistics are based on $N = 102$ events which fulfil the condition $|p| \geqslant 3p_{rms}$, and the mean characteristic time was found to be $\overline{T}_{ch} = 2.3$ ms. From the reciprocal characteristic time, a characteristic frequency $\bar{f} = 1/\overline{T}_{ch}$ is obtained with $\bar{f} = 430$ Hz ($\omega^+ = 0.52$). If one compares this characteristic

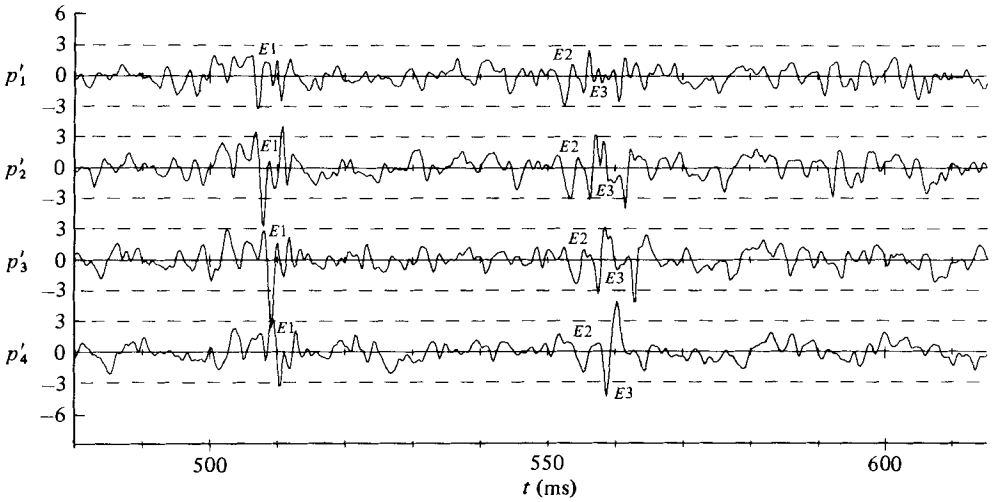

FIGURE 13. Time functions of four consecutive pressure transducers (the amplitudes p_i are normalized to their p_{rms}, distance $\xi = 4$ mm, $\xi^+ = 75$).

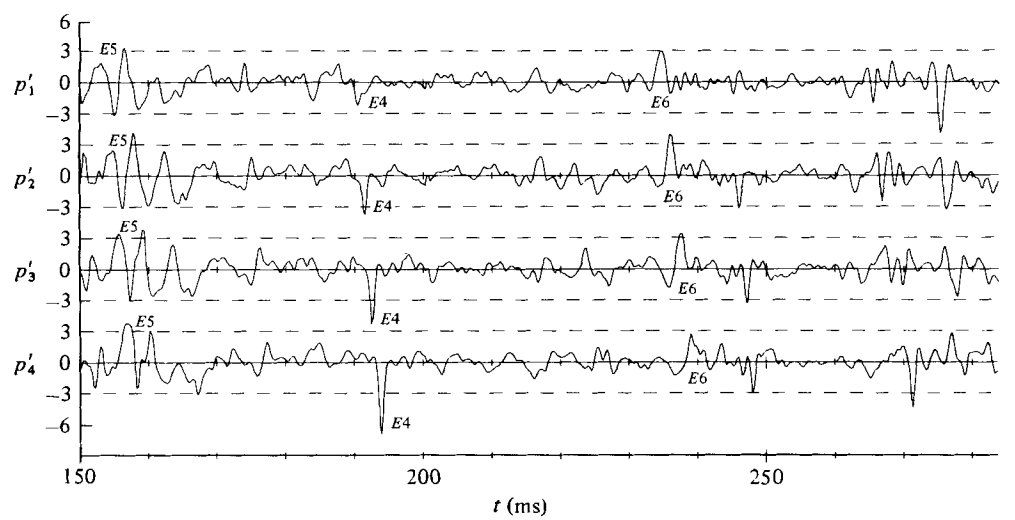

FIGURE 14. Same notation as in figure 13.

frequency $\omega^+ = 0.52$ with the burst frequency ω_{B} observed by Kim, Kline & Reynolds (1971), one finds that the value $\omega_{\mathrm{B}}^+ (Re = 1400) = 0.05$ is one order of magnitude smaller than the characteristic frequency of the pressure structures with high amplitude. Furthermore, it is interesting to remember the extrapolated slope constant of the power-spectral density with a value of $\omega_{\mathrm{SL}}^+ = 0.26$, which is half of the characteristic frequency $\omega^+ = 2\omega_{\mathrm{SL}}^+$. The question whether this relation is generally valid cannot be answered because the flow parameters remained constant throughout all measurements.

7.2. *Analysis by signal averaging*

Apart from a visual analysis, the signal-averaging procedure in the time domain is a suitable method to detect common features of the characteristic pressure structures.

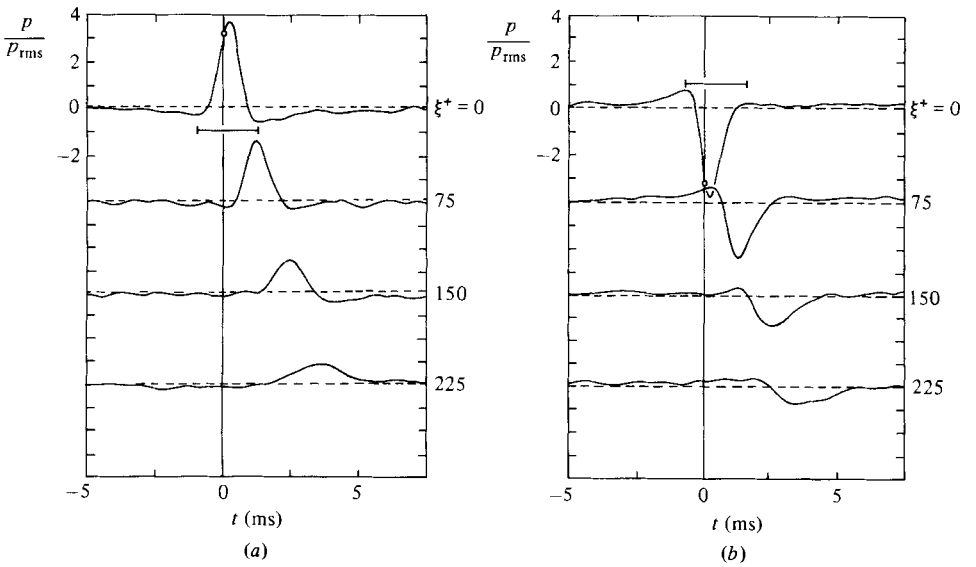

FIGURE 15. Analysis of characteristic pressure structures with high amplitude by 2-channel 'signal averaging' (symbol ○ indicates triggering point, ξ^+ distance between the two transducers): (*a*) positive threshold = $3.2p_{\rm rms}$; (*b*)' negative threshold = $-3.2p_{\rm rms}$.

With a Nicolet 2-channel analyser (660A), pairs of the 4-channel wall-pressure measurements (stored on analog magnetic tape) were investigated. By a given triggering level for the first channel, the events and their temporal surroundings were selected and then stored in the memory bank. The events were scanned with 1024 points per channel, where the triggering point in the first channel always corresponded to the 512th point of time. Thus the instant the trigger threshold is exceeded in the first channel, the temporal point of reference is defined at which all events are averaged in both channels. Through point-by-point addition of the individual time segments and subsequent division by the number of the segments, an averaged curve is obtained for both channels. For the triggering level, a positive as well as a negative threshold of $3.2p_{\rm rms}$ was used.

Results of three individual measurements are illustrated in figure 15(*a*) for the positive threshold. These three measurements are obtained by the three possible intervals $\xi^+ = \Delta x u_\tau/\nu$ where reference was taken each time to the first pressure transducer $\xi^+ = 0$. Figure 15(*b*) shows the corresponding measurements for the negative threshold. The triggering point lies at $t = 0$, and the averaged amplitudes for $\xi^+ = 0$, according to the definition, amounted to $p = \pm 3.2p_{\rm rms}$. During all tests it was attempted as far as possible to analyse the same tape segment. Owing to the limited capacity of the analyser to detect immediately consecutive events, the final counts may be considered to provide only a qualitative statement. The positive threshold was exceeded 178 times and the negative threshold 236 times, whereby the occurrence of non-Gaussian effects – the measured negative skewness of the probability distribution (figure 5 and 6) – is confirmed.

The averaged signal curves are pulselike peaks with a rather strong tendency to overshoot. This tendency is caused by the fact that the events of high amplitude have the features of very short wavetrains. Through visual analysis of the 102 individual events it became apparent that an event usually consists of two or more extremes of alternating signs. Both curves for $\xi = 0$ in figure 15 allow evaluation with reference

to their characteristic time. For the sake of comparison the characteristic time $\bar{T}_{ch} = 2.3$ ms, determined by visual analysis, is included in both figures and is thus clearly confirmed. Quantitative determination of the characteristic time by means of the averaged signal curve alone appears inaccurate, since the shape of the averaged curve is dependent on the fixed trigger level used for the selection of the events.

These measurements allow a statement to be made concerning the convective behaviour of the characteristic pressure structures. It is obvious that, with an increasing distance between the two pressure transducers, the width of the peaks increases as well, while the centroid of the area of the peaks is shifted in time t in proportion to the distance ξ^+. From the respective distance ξ^+ and the corresponding time shift t of the centroid of the area, a convection velocity $u_c = 0.53u_\infty = 11.9u_\tau$ is determined for the characteristic pressure structures. There are two reasons for the increase in width of the peaks: the first is the decay of the events on the way between the two transducers, the second is the different convection velocity of the individual events. The decay of the maximum amplitude with increasing distance ξ^+ is approximately exponential for both thresholds. In Kreplin & Eckelmann (1979) the mean propagation velocity of perturbations in the viscous sublayer was determined by space–time correlations of the velocity gradient at the wall. They measured a convection velocity $c_x = 12.1u_\tau$ for both the streamwise and spanwise fluctuations at the wall. This value is nearly the same as the convection velocity of the characteristic pressure structures of the present investigations. From the characteristic frequency $\bar{f} = 430$ Hz ($\omega^+ = 0.52$), which was obtained by visual analysis, a characteristic wavelength of $\lambda^+ = 145$ ($\lambda/\delta^* = 1.7$) results owing to the fact that $f = u_c/\lambda$.

In Schewe (1979) a value of $\lambda^+ = 170$ was determined, which was obtained as the result of correlation measurements of the wall pressure gradient. Considering the difficulty of defining and determining such characteristic values the difference seems to be insignificant. Nevertheless, the wavelength $\lambda^+ = 145$ appears to be valid because the present method of determination of the convection velocity is more appropriate than in the previous investigation.

Finally it should be remarked that λ^+ is not an integral lengthscale but the mean distance between two consecutive extremes with the same sign for the x-direction of the instantaneous spatial pressure distribution. Thus for the characteristic pressure structures the distance between a maximum and a consecutive minimum is $\frac{1}{2}\lambda^+ = 73$, which is less than or approximately equal to the smallest transducers used in previous measurements (again pinhole measurements have not been taken into consideration).

To summarize, the characteristic pressure structures with high amplitude have the mean values $\omega^+ = 0.52$, $\lambda^+ = 145$ and their mean convection velocity amounts to $u_c/u_\infty = 0.53$.

8. Discussion of the results

If infrequently-appearing structures are found in the time functions of a physical process, then the question arises as to the meaning of these structures in the process as a whole. Upon examination of the probability distribution (figure 6) it is obvious that the occurrence of events with $|p| \geqslant 3p_{rms}$ has low probability, and thus the power spectrum (figure 8) shows that the characteristic frequency $\omega^+ = 0.52$ lies within the region of decay. Conversely, when the contribution of these events to the r.m.s. value is calculated, it becomes clear that they play an important role in the wall region of the turbulent boundary layer. In addition, it was calculated from the probability distribution that these events contribute 40% to the r.m.s. pressure, although the

threshold $\pm 3p_{\mathrm{rms}}$ is exceeded only 1 % of the time. The determination of time fractions is explained in § 4. The contribution to the r.m.s. value of the events which exceed the threshold was calculated with the help of the following relation:

$$\overline{p^2} = \int p^2 W(p)\,\mathrm{d}p.$$

If, for the sake of comparison, a Gaussian distribution is applied instead of the measured probability distribution of the wall-pressure fluctuations, then the contribution to the r.m.s. value is 17 % at the same threshold value of $\pm 3p_{\mathrm{rms}}$ which is exceeded 0.3 % of the time.

Since the wall-pressure fluctuations are related to the velocity fluctuations in the boundary layer, it is of interest to guess the average wall distance for the sources of the characteristic wall-pressure structures. Assuming that these sources move with mean local velocity within the boundary layer, it follows from the velocity profile (figure 1) that the wall distance is $y^+ = 21$ with $u_c = 0.53u_\infty = 11.9u_\tau$. Another interesting possibility is to refer to the visual and anemometric measurements of Hofbauer (1978), who detected three-dimensional instability waves in the velocity field of a turbulent channel flow. The frequency and amplitude of these waves were a function of the wall distance y^+. Hofbauer found that the angular frequency ω of these instability waves is equal to the local derivative of the mean velocity profile $\partial\bar{u}/\partial y$. Thus it is possible with the knowledge of the frequency to determine the approximate region of the origin of the characteristic pressure structures. If we assume that the pressure fluctuations are dependent on linear and quadratic terms of the velocity fluctuations, the following rough approximation can be made: in the case that linear terms dominate ($p \sim u$), a wall distance of $y^+ = 12$ is obtained from Hofbauer's measurement of $\omega^+(y^+)$. In the case that quadratic terms dominate ($p \sim u^2$), then a wall distance of $y^+ = 20$ is found. Thus both methods, evaluation of the velocity profile and use of Hofbauer's results, lead to the wall range $12 \lesssim y^+ \lesssim 21$ as the region of origin for the characteristic pressure structures. This region of origin $y^+ \approx 10$–25 lies in the buffer layer, which is the transition region from the linear to the logarithmic part of the velocity profile. This region is distinguished by several marked features, which are probably due to the fact that the occurrence of a burst is most probable within this region, as discovered by Kim *et al.* (1971). According to Hofbauer (1978), the maximum of the turbulence production lies within this region (particularly at $y^+ = 12$), and the statistical moments of the u-fluctuations have pronounced values: the r.m.s. value is maximal, the skewness factor has a zero-crossing and the flatness factor is minimal.

The test results, obtained with pressure transducers of various sizes (diameters ranging around a factor of 18), can also be explained by the occurrence of the characteristic pressure structures. If a spatial low-pass filtration is achieved by enlarging the pressure transducers, the r.m.s. value falls to half its previous value and the probability distribution converges to a Gaussian distribution. Upon close observation of the curve illustrating the dependence of the r.m.s. value on the pressure transducer diameter, it is obvious that the curve rises gradually from $d^+ = 333$ (largest diameter) up to $d^+ \approx 165$. For smaller diameters $d^+ < 165$ the increasing slope is linear and steeper than for $d^+ > 165$. Since the characteristic pressure structures have a characteristic wavelength of $\lambda^+ = 145$ the resolution increases with decreasing d^+ especially in the region $d^+ < 145$. The diameter of the smallest pressure transducer ($d^+ = 19$) is almost eight times smaller than $\lambda^+ = 145$. Conversely if the pressure transducer's diameter is larger than $d^+ = 145$, then the characteristic pressure

structures are nearly spatially filtered out. According to this explanation, it can be stated that for wall pressure fluctuations the deviation from the Gaussian distribution is caused by the characteristic pressure structures with high amplitudes.

The author would like to thank the Director of the Institute, Prof. Dr E.-A. Müller, for providing the opportunity to carry out the investigation and for his interest in it. Gratitude is expressed particularly to Dr A. Dinkelacker for initiating this investigation and for his continuous support. Thanks go to Dr M. Hofbauer for many discussions and suggestions in difficult phases and to Dr H. Eckelmann, who read the manuscript and made helpful suggestions. The important contribution of Dr K. H. Zimmermann, who developed the amplifiers for the transducers, also deserves acknowledgement. Finally, the author is indebted to the constructive criticism of the referees.

REFERENCES

BLAKE, W. K. 1970 *J. Fluid Mech.* **44**, 637–660.
BULL, M. K. 1967 *J. Fluid Mech.* **28**, 719–754.
BULL, M. K. & THOMAS, A. S. W. 1976 *Phys. Fluids*, **19**, 597–599.
CANTWELL, B. J. 1981 *Ann. Rev. Fluid Mech.* **13**, 457.
CORCOS, G. M. 1963 *J. Acoust. Soc. Am.* **35**, 192.
CORCOS, G. M. 1967 *J. Sound Vib.* **6**, 59–70.
DINKELACKER, A., HESSEL, M., MEIER, G. E. A. & SCHEWE, G. 1977 *Phys. Fluids* **20**, 216–224.
ECKELMANN, H., NYCHAS, S. G., BRODKEY, R. S. & WALLACE, J. M. 1977 *Phys. Fluids* **20**, 225–231.
EMMERLING, R. 1973 *Mitt. MPI f. Strömungsforschung & AVA Göttingen* no. 56.
EMMERLING, R., MEIER, G. E. A. & DINKELACKER, A. 1974 *AGARD Conf. Proc.* no. 131, 24-1–24-12.
HESSEL, M. 1978 *Rep. MPI f. Strömungsforschung, Göttingen* no. 11/1978.
HODGSON, T. H. 1962 PhD thesis, London University.
HOFBAUER, M. 1978 *Mitt. MPI f. Strömungsforschung & AVA Göttingen* no. 66.
HOFBAUER, M. 1979 *AGARD Rep.* no. 271.
KIM, H. T., KLINE, S. J. & REYNOLDS, W. C. 1971 *J. Fluid Mech.* **50**, 133–160.
KREPLIN, H. P. & ECKELMANN, H. 1979 *J. Fluid Mech.* **95**, 305–322.
KUHL, W., SCHODDER, G. R. & SCHRÖDER, F.-K. 1954 *Acustica* **4**, 519–532.
MONIN, A. S. & YAGLOM, A. M. 1975 *Statistical Fluid Mechanics*, vol. II. MIT Press.
LANGEHEINEKEN, T. & DINKELACKER, A. 1978 *Fortschritte der Akustik*, p. 391. VDE-Verlag.
SCHEWE, G. 1979 *Mitt. MPI f. Strömungsforschung Göttingen* no. 68A.
SCHEWE, G. 1980 *Rep. MPI f. Strömungsforschung, Göttingen* no. 1/1980.
WILLMARTH, W. W. 1975 *Ann. Rev. Fluid Mech.* **7**, 13–38.
WILLMARTH, W. W. & ROOS, F. W. 1965 *J. Fluid Mech.* **22**, 81–94.